International Journal of Fracture (2006) 140:3–14
DOI 10.1007/s10704-006-6579-2

Nanoscale damage during fracture in silica glass

D. BONAMY[1,*], S. PRADES[1,2], C. L. ROUNTREE[1,3], L. PONSON[1], D. DALMAS[1,4], E. BOUCHAUD[1], K. RAVI-CHANDAR[5] and C. GUILLOT[1]
[1]*Fracture Group, Service de Physique et Chimie des Surfaces et Interfaces, DSM/DRECAM/SPCSI, CEA Saclay, F-91191 Gif sur Yvette, France*
[2]*Present address: Department of Materials, Swiss Federal Institute of Technology, ETH Hönggerberg, Wolfgang-Pauli-Strasse 10 CH-8093 Zürich, Switzerland*
[3]*Collaboratory for Advanced Computing and Simulations, Departments of Material Science and Engineering, Physics and Astronomy, Computer Science and Biomedical Engineering University of Southern California, Los Angeles, CA 90089-0242, USA*
[4]*Present address: Glass Surface and Interface, Unité Mixte CNRS/Saint-Gobain, F-93303 Aubervilliers Cedex, France*
[5]*Center for Mechanics of Solids, Structures and Materials, Department of Aerospace Engineering and Engineering Mechanics, University of Texas, Austin, TX 78712, USA*
[*]*Author for correspondence (E-mail: bonamy@drecam.cea.fr)*

Received 6 July 2005; accepted in revised form 6 January 2006

Abstract. We report here atomic force microscopy experiments designed to uncover the nature of failure mechanisms occuring within the process zone at the tip of a crack propagating into a silica glass specimen under stress corrosion. The crack propagates through the growth and coalescence of nanoscale damage spots. This cavitation process is shown to be the key mechanism responsible for damage spreading within the process zone. The possible origin of the nucleation of cavities, as well as the implications on the selection of both the cavity size at coalescence and the process zone extension are finally discussed.

Key words: AFM, brittle fracture, corrosion fatigue, damage.

JEL codes: D24, L60, 047.

1. Introduction

Silicate glasses are often considered as the archetype of brittle materials. It is commonly thought (Kelly et al., 1967; Lawn et al., 1980; Guin and Widerhorn, 2004) that its fracture is similar to cleavage – with a crack progressing through sequential bond ruptures without involving any damage ahead of the crack tip. However, some recent observations call into question this scenario:

- The morphology of fracture surfaces in glasses exhibits scaling features similar to the ones observed in a wide range of quasi-brittle and ductile materials, e.g. oxide glass, polymers, metallic alloys, wood, rocks… (see Bouchaud, 1997 and references therein). This strongly suggests the existence of some underlying generic mechanisms within the process zone common to all these materials.
- The deformation field was shown not to fit with the linear elastic predictions over a fairly large region (of the order of a hundred of nanometers) in the vicinity of the crack tip (Guilloteau et al., 1996; Hénaux, and Creuzet, 2000).

– Molecular Dynamic (MD) simulations indicate that fracture in silica glass proceeds through the growth and coalescence of nanoscale cavities (Van Brutzel et al., 2002; Rountree et al., 2002; Kalia et al., 2003).

These various results have led us to investigate experimentally the failure mechanisms occurring in glass at its microstructure scale, the nanoscale. The first series of experiments, reported in Célarié et al. (2003a,b) and Marlière et al. (2003), were carried out on aluminosilicate vitroceramics. They clearly reveal that crack progresses through the growth and coalescence of nanoscale damage cavities. We describe here our recent studies performed on a minimal elastic vitreous medium, pure silica. The experimental setup is described in Section 2. In Section 3, we present the experimental results. As in the aluminosilicate vitroceramics, crack propagation proceeds through the nucleation, growth and coalescence of damage cavities (Section 3.1). The rate of cavity nucleation and the size of cavities at coalescence are shown to set the mean crack growth velocity as measured at the continuous scale (Section 3.2). This nanocavitation process is shown to set the process zone size (Section 3.3). Finally, Section 4 is devoted to a discussion on a possible scenario explaining the existence of damage cavities ahead of the crack tip, and its implications as regard to the cavity size at coalescence (Section 4.1) and the process zone size (Section 4.2).

2. Experimental setup

The experimental set-up has been described in detail in Prades et al. (2005a) and is briefly recalled below. Fracture was performed on double cleavage drilled compression parallelepipedic samples (size $5 \times 5 \times 25\,\mathrm{mm}^3$) with a cylindrical hole drilled in the center (radius 0.5 mm). A gradually increasing uniaxial compressive load was applied to the sample (Figure 1). Once the two cracks are initiated symmetrically from the hole, the load is held constant. In this geometry, the stress intensity factor K_I can be related to the crack length using the expression given by He et al. (1995).

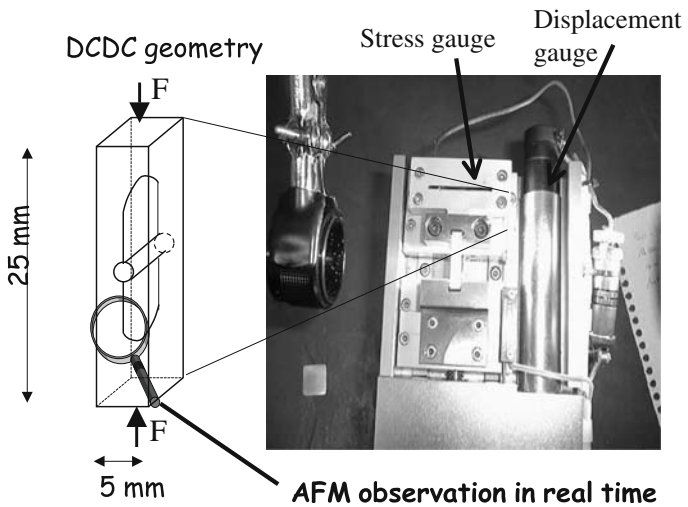

Figure 1. Experimental setup showing the loading DCDC configuration used to fracture the glass specimen under stress corrosion.

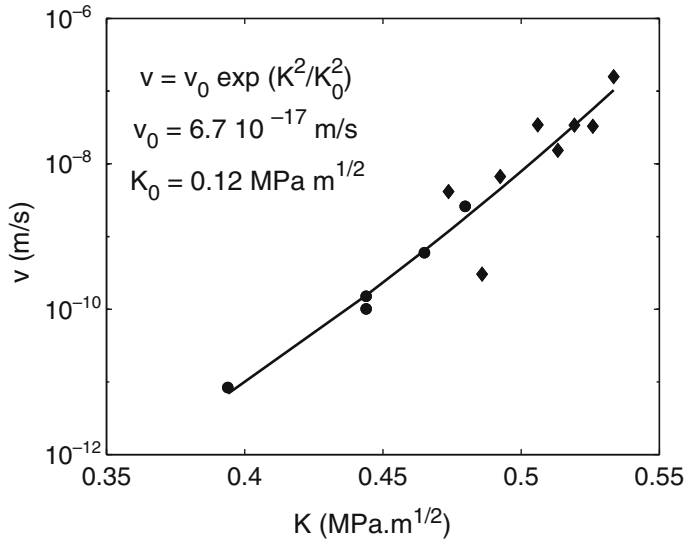

Figure 2. Variation of the mean crack growth velocity v (in $\mathrm{m\,s^{-1}}$) as a function of the stress intensity factor K_I (in $\mathrm{MPa\,m^{1/2}}$). The axes are semi-logarithmic. Diamonds and dots correspond to optical and AFM measurements, respectively. The line is a fit using $v = v_0 \exp(K_\mathrm{I}^2/K_0^2)$ as expected for stress enhanced activated process models.

While the cracks length increases, K_I decreases. Under vacuum, the crack would stop when K_I gets smaller than the material fracture toughness K_Ic. But, in our room atmosphere (relative humidity 45%, temperature 26 °C), the corrosive action of water on glass allowed slow, sub-critical, crack propagation. The crack tip advance was then slow enough to be probed by AFM.

The crack growth velocities v considered in this study range between 10^{-12} and 10^{-6} m/s. In this velocity range, v increases exponentially with K_I^2 (Figure 2) in agreement with stress enhanced activated process models proposed by Wiederhorn (1967) and Wiederhorn and Boltz (1970). The velocity could then be tuned by adjusting the external applied load for a measured crack length. It was varied over three decades, from 10^{-9} and 10^{-12} m/s (the maximum reachable velocity being set by the recording time of an AFM frame, around 3 min).

In all the following, the reference frame $(\vec{e}_x, \vec{e}_y, \vec{e}_z)$ is chosen so that $\vec{e}_x$, $\vec{e}_y$ and $\vec{e}_z$ are parallel to the crack propagation, tension loading at the crack tip and sample thickness directions, respectively.

3. Experimental results: damage spreading mechanisms within the process zone

3.1. Evidence of damage cavities ahead of the crack tip

Our experimental setup has allowed to observe the crack progression within the process zone in real time at the nanoscale. Figures 3 (a)–(f) show six successive AFM topographic frames in the vicinity of the crack tip in pure silica glass. For this specific sequence, the crack propagates at an average velocity $v \simeq 4 \times 10^{-11}$ m/s. One can clearly see a depression ahead of the crack tip. This cavity grows to a typical size

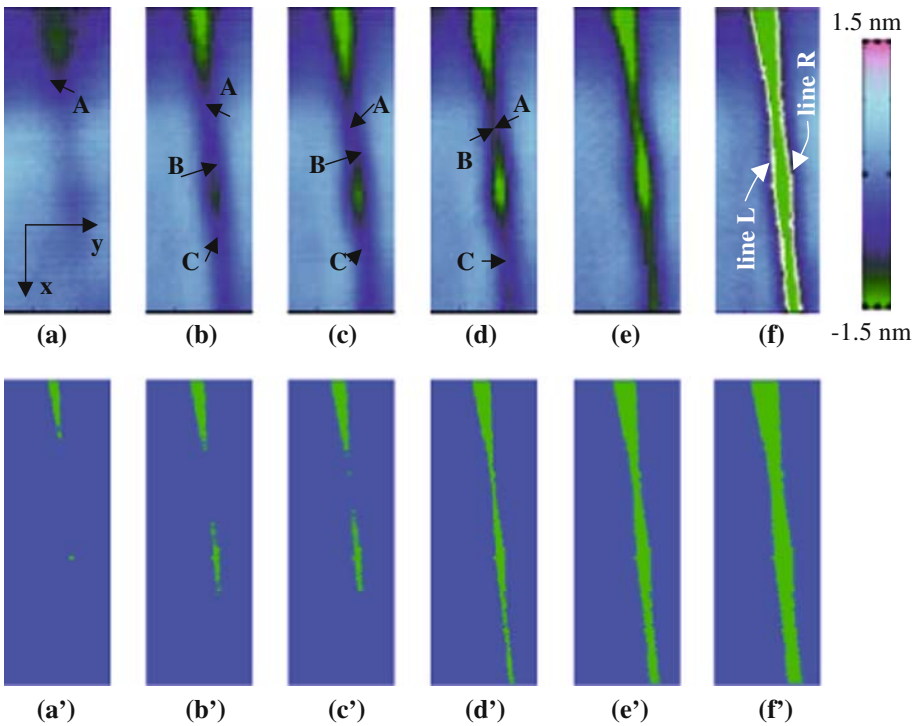

Figure 3. (a)–(f) Sequence of topographic AFM frames in the vicinity of the crack tip showing the propagation of the crack in stress corrosion regime ($v = 4 \times 10^{-11}$ ms^{-1}). The scan size is 470×135 nm^2 and the height range over 3 nm. The six frames were taken during the five hours necessary for the main crack to cross the area of interest. (a,b) Appearance of a nanometric damage cavity ahead of the crack tip, (b–d) growth of the cavity prior to crack propagation and (f,g) coalescence of the cavity with the main crack. The points A, B and C locate the position of the main CT, the BF and the FF tips of the cavity, respectively. (a′)–(f′) reconstructed frames using the FRASTA method.

of 100 nm in length and 20 nm in width, and then merges with the advancing main crack to make it cross the whole area of observation. In other words, the crack front does not propagate regularly as commonly stated (Kelly et al., 1967; Lawn et al., 1980; Guin and Wiederhorn, 2004), but progresses through the growth and coalescence of cavities. This scenario is fully consistent with what was observed both experimentally in aluminosilicate vitroceramic under stress corrosion by Célarié et al. (2003a,b) and Marlière et al. (2003) (Figure 4(bottom)) and numerically in dynamic fracture of amorphous silica by Van Brutzel et al. (2002), Rountree et al. (2002) and Kalia et al. (2003) (Figure 4(top)).

Fracture Surface Topography Analysis (Kobayashi et al., 1987; Miyamoto et al., 1990) was then performed to ensure that the spots observed ahead the crack tip correspond actually to damage cavities. In a ductile scenario, the growth of damage cavities is expected to induce irreversible plastic deformations that will leave visible prints on the *post-mortem* fracture surfaces. We have thus determined the fracture lines after the crack has crossed the area of interest (white lines in Figure 3f) and reconstituted virtually the intact material by placing the line on the right – line R – to the left of the line on the left – line L (Bonamy et al., 2005 submitted). By translating gradually the line R to the right, one reproduced qualitatively the chronology of

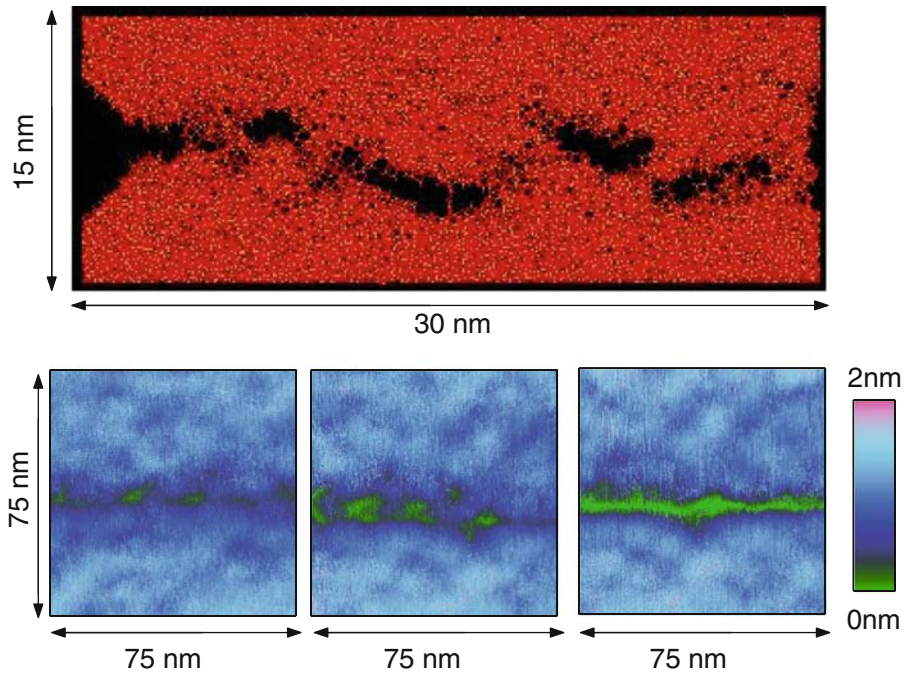

Figure 4. Top: Snapshots of atoms as observed in a MD simulation of dynamic fracture in amorphous Silica (from van Brutzel, 1999). Bottom: Sequences of three sucessive AFM snapshots showing the vicinity of the CT at the surface of an aluminosilicate glass specimen (from Célarié et al., 2003a,b). In both cases, the crack progresses through the growth and coalescence of damage cavities.

the cavity growth (Figure 3(a′)–(f′)). This provides a rather strong argument to relate these nano-scale spots to damage cavities.

It is worth to note that the reconstructed cavity is found to be thinner than the real one. This can be understood as follows: The shape of the real cavity is given not only by the irreversible – permanent – part of the opening displacements at the free surface, but also by the reversible – elastic deformation –. This latter decreases when the crack progresses outside the area of interest since the stresses partially relax. The elastic contribution is then taken into account *only partially* in the reconstructed frames (Bonamy et al., 2005 submitted). As a consequence, the remnants of these nanospots growing ahead of the crack tip on the post-mortem fracture surfaces are expected to be much smaller – and thus much harder to detect – than the spots themselves. This may explain why Guin and Wiederhorn (2004) did not succeed to see evidences of the pores' remnants from the analysis of the mismatch between the two opposite post-mortem fracture surfaces.

3.2. Kinematics of damage cavities

From the sequences represented in Figure 1(a)–(f), the temporal evolutions of the main crack tip (CT), the forward front tip (FF) and the backward front tip (BF) of the cavity were then determined, and the corresponding velocities extracted (Figure 5). These velocities were found to be $v^{\mathrm{CT}} = 4 \times 10^{-12}$ m/s, $v^{\mathrm{FF}} = 1.1 \times 10^{-11}$ m/s and $v^{\mathrm{BF}} = 1.2 \times 10^{-11}$ m/s for the main CT, the FF and the BF of the cavity, respectively, i.e. significantly smaller than the mean CT velocity $v = 4 \times 10^{-11}$ m/s as

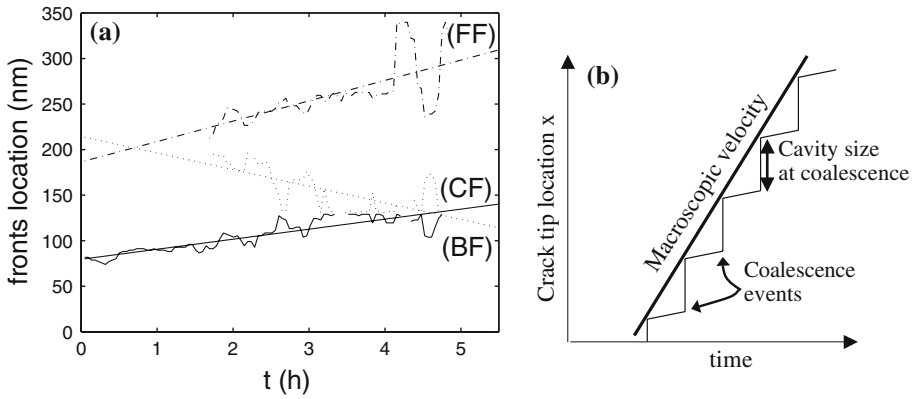

Figure 5. (a) Temporal evolution of the main crack front (CF) and the BF of the cavity and the FF of the cavity represented by points *A*, *B* and *C* on the frames of Fig. 3(a)–(e), respectively. The velocities of these fronts are determined through linear fits: $v^{\mathrm{CF}} \simeq 4 \times 10^{-12}\,\mathrm{ms}^{-1}$, $v^{\mathrm{BF}} \simeq 1.2 \times 10^{-11}\,\mathrm{ms}^{-1}$ and $v^{\mathrm{FF}} \simeq 1.1 \times 10^{-11}\,\mathrm{ms}^{-1}$. The thicker line shows the velocity at the continuum scale: $\langle v \rangle \simeq 4 \times 10^{-11}\,\mathrm{ms}^{-1}$. (b) Sketch of the CT propagation at the scale of the process zone.

measured optically (Prades et al., 2005a). In other words, the crack growth velocity as observed at the continuum scale is dominated by the accelerating phases corresponding to cavity coalescence with the main crack front.

3.3. Nanocavitation and process zone

We then determined the extension of the process zone (Bonamy et al., 2005 submitted; Prades et al., 2005b submitted). Linear Elastic Fracture Mechanics (LEFM) predicts that the stress field exhibits a universal square root singularity at the CT in an intact linear elastic medium. One thus expects a square root singularity in the components of the stress tensors, and in the out-of-plane displacement at the free surface of the specimen. The surface topography was thus imaged in the vicinity of the CT (Figure 6a), and compared to the LEFM predictions (Figure 6b). Far from the CT, one recovers the LEFM predictions. But below a given threshold, the experimental curves depart from the predictions. This departure point sets the extent of the process zone (Guilloteau et al., 1996; Célarié et al., 2003a). This extension was found to be around 100–300 nm in length (x-direction) and around 20 nm in width (y-direction) in the stress corrosion experiment (v ranging from 8×10^{-12} to 10^{-9} m/s) (Bonamy et al., 2005; Prades et al., 2005b). It was found to be significantly smaller, around 10–25 nm in length, and 7–11 nm in width for the MD simulation of dynamic crack propagation (v ranging from 10 to 400 m/s) (Prades et al., 2005b submitted). Let us finally note that similar signature of non elastic behaviour within the 100 nm range in the vicinity of a crack tip was evidenced by Hénaux and Creuzet (2000) in amorphous Silica under stress corrosion by comparing the crack opening displacements measured experimentally to the one predicted from linear elasticity.

We finally compared the extension of the process zone as defined above to the extent of the zone made "porous" in the vicinity of the crack due to the presence of cavities. Those were shown to coincide (Prades et al., 2005b submitted). This

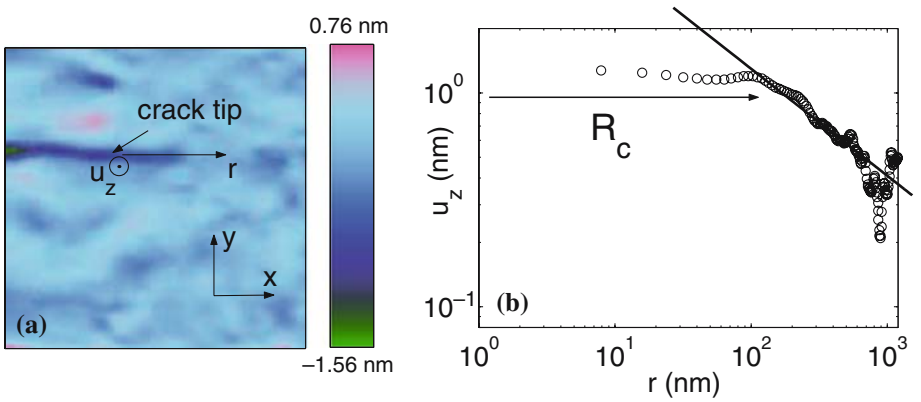

Figure 6. Measurement of the extension of process zone. (a) $1 \times 1\mu$m AFM topographical frame of the vicinity of the CT. The crack growth velocity was $v \simeq 1.5 \times 10^{-10}$ m/s (b) Variation of the out-of-plane displacement u_z as a function of the distance r from the CT measured along the direction of crack propagation (x-axis). The axes are logarithmic. The straight red line corresponds to the LEFM predictions. For r smaller than a given value $R_c \simeq 150$ nm, the experimental curve departs from the LEFM predictions. This value sets the extent of the process zone along the x-direction for this specific experiment.

indicates that nucleation and growth of cavities provide the dominant mechanism responsible for damage spreading within the process zone.

4. Discussion: on the relevant lengthscales

Observations of damage cavities in amorphous silica under stress corrosion are consistent with what was observed experimentally in aluminosilicate vitroceramics under stress corrosion by Célarié et al. (2003a,b) and Marlière et al. (2003), and numerically during dynamic failure of amorphous silica by Van Brutzel et al. (2002), Rountree et al. (2002) and Kalia et al. (2003). This indicates that the origin of such a nanoscale damage mode is inherent to the amorphous structure and does not depend on the precise glass composition. Origin of the damage cavities should be found in the amorphous structure, which contains *inherent density and/or residual stress fluctuations at the nanoscale*. This results in "less tough" regions ahead of the crack tip where bonds can be broken before the ones at the CT (Figure 7a). These nucleation points behave as stress concentrators and grow under the stress imposed by the presence of the main crack to give birth to micro-cracks (Figure 7b). The stress field then stops being dominated by the square root singularity in the very vicinity of the CT because of the screening due to these micro-cracks. This set the process zone. It should be emphasized that the stress level remains significantly smaller than the yield stress σ_y and the material remains linearly elastic almost everywhere within this process zone, except in the very vicinity of the various tips (main CT and tips of the micro-cracks) where it concentrates and reaches the yield stress value σ_y (Figure 7b). Tips blunting then occurs and the micro-cracks become damage cavities that will leave remnants on the porst-mortem fracture surface once the stress field has relaxed (Figure 7c).

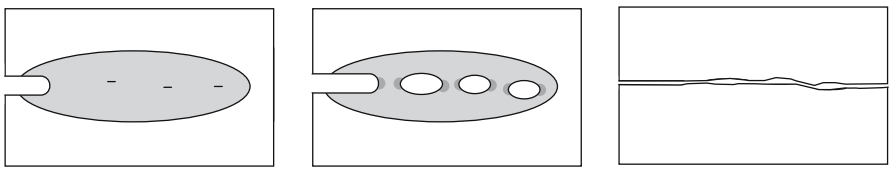

Figure 7. Conjectured scenario for damage spreading within the process zone in Silica glass: Amorphous structure of the material results in regions with low density and/or higher residual stress where bonds will break before the ones at the crack tip (Figure a). These nucleation points behave as stress concentrators and grow under the stress imposed by the presence of the main crack to give birth to micro-cracks (Figure b). The stress field within the process zone (pale gray in figure b) is then given by the complex combination of the stress concentration at the main CT and at the tip of all the cavities – all of them interacting with each others. The stress level remains below the yield stress, except in the very vicinity of the crack and cavities tips (dark gray in figure b). Tips blunting occurs there at sub-nanometric scale, which leaves remnant on the porst-mortem fracture surface once the stress field has relaxed (Figure c).

4.1. Cavity size at coalescence

In this scenario, the typical size of the damage cavities can be understood as follows. Intrinsic amorphous fluctuations induce low toughness regions with a density ρ_0 of bonds that can be broken ahead of the CT. In dynamic fracture, the stress within the process zone is sufficient to activate any of these "low toughness sites". The typical distance between two nucleation sites – and consequently the typical size of cavities at coalescence – is given by the lengthscale δ_0 of the fluctuations induced by the amorphous structure. Since δ_0 is of the order of the nanometer, one expects a cavity size of the order of one nanometer which is compatible with the MD observations (Van Brutze et al., 2002; Rountree et al., 2002; Kalia et al., 2003).

This scenario can be extended to the stress corrosion regime (Prades et al., 2005b submitted.) In that case, the stress level in the process zone is too low to make low toughness sites give birth to damage cavities. However, the corrosive action of water activates some of them. The probability ρ/ρ_0 – where ρ refers to the density of activated sites – is expected to scale as $\rho/\rho_0 \propto \exp(\alpha G/kT)$ where α, G, k and T refer to a typical activation area, the mechanical energy within the process zone, the Boltzmann constant, and the temperature, respectively. Since the crack growth speed v scales also as $v \propto \exp(\alpha G/kT)$ (Wiederhorn, 1967; Wiederhorn and Boltz 1970; Prades et al., 2005a), one gets $\rho/\rho_0 \propto v$. The typical distance δ between two nucleation points – and consequently the typical size of the cavity at coalescence – scales as $\delta \propto \rho^{-1/3}$. Hence $\delta/\delta_0 \propto v^{-1/3}$. In glasses under stress corrosion, crack growth stops being dominated by the rate of hydrolysis chemical reactions when v is greater than a threshold v^* classically described as the limit between stress corrosion regions I and II in the literature (Wiederhorn, 1967; Wiederhorn and Boltz, 1970; Lawn, 1993). The corresponding mechanical energy $G(v = v^*)$ is thus expected to be sufficient to activate all the low toughness sites: $\delta(v = v^*) \simeq \delta_0$. Finally, one gets $\delta/\delta_0 \simeq (v/v^*)^{-1/3}$ in the ultra-slow stress corrosion regimes. For our experimental conditions (relative humidity 45%, temperature 26 °C), $v^* \simeq 10^{-5}$ m/s (Wiederhorn, 1967; Wiederhorn and Boltz, 1970; Lawn, 1993). Since $\delta_0 \simeq 1$ nm, one gets $\delta \simeq 100$ nm for $v \simeq 4 \times 10^{-11}$ m/s, which is in good agreement with observations (Figure 3).

4.2. Size of the process zone

The value of intrinsic strength of Silica glass measured in vacuum at room temperature, is around $\sigma^* \simeq 10-12$ GPa (Kurkjian et al., 2003) and the fracture toughness is about $K_{Ic} \simeq 1\,\mathrm{MPa\,m^{1/2}}$. With these properties we can estimate the fracture process zone to be about $(K_{Ic}/\sigma^*)^2/3 \simeq 1-2\,\mathrm{nm}$ based on LEFM (Irwin, 1957; Dugdale, 1960; Barenblatt, 1962). However, the experiments reported here were performed under subcritical conditions, in a stress corrosion environment, at a stress intensity factor of $K_I \simeq 0.5\,\mathrm{MPa\,m^{1/2}}$. LEFM estimate shows that the stress is smaller than 12 GPa for distances larger than 30 $\mathring{A}$ from the CT; thus, instantaneous fracture does not occur. The fracture process in the Silica glass under conditions considered here is one of damage accumulation under sub-critical loading. However, sub-critical crack growth occurs through stress corrosion and it must be noted that damage can accumulate over a significantly large region near the CT; in order to estimate the size over which this occurs, we use two significant observations. First, Proctor et al. (1967) found the intrinsic strength of Silica glass in humid air to be significantly smaller, around $3-4\,\mathrm{GPa}$, hence damage through stress corrosion could occur at stress levels that are of this order, anywhere in the vicinity of the CT as long as moisture is present. Second, molecular dynamics analysis by Swiler et al. (1995) suggests the presence of voids as large as 0.45 nm in unstressed silica glass. These voids will concentrate the stress in their vicinity, by a factor of 3 or more depending on the aspect ratio of the voids (lnglis, 1913). Thus, damage accumulation near the crack tip may occur at distances where the stress is elevated to about $\sigma \simeq 1\,\mathrm{GPa}$ or perhaps smaller. This generates the appropriate fracture process zone size and is counterintuitive in that it can be larger than the process zone generated under monotonic loading to failure! Once again using LEFM the damage zone can be estimated to be on the order of about $Rc \simeq (K_\mathrm{I}/\sigma)^2/3 \simeq 80\,\mathrm{nm}$. This order of magnitude is compatible with what was measured from the AFM topography (Figure 6), particularly on the surface where diffusion of water molecules is not constrained by the bulk diffusion of water in glass.

One may however wonder how water molecules can travel from the CT along such a large distance within the glass. For water to travel over this distance in typically an hour, it requires a diffusion coefficient $D \simeq 10^{-14}\mathrm{cm^2 s^{-1}}$ (Bonamy et al., 2005 submitted) fives orders of magnitude larger than what is commonly observed in the absence of stress ($D \simeq 10^{-19}\,\mathrm{cm^2 s^{-1}}$). However, Tomozawa et al. (1991) have shown that water diffusion can be grealty accelerated under stress. By using $^{15}\mathrm{N}$ resonant nuclear reaction technique, they measured the depth profiles of hydrogen concentration on fracture surfaces of Silica glass obtained by (i) stress corrosion cracking in a DCDC specimen immersed in distilled water and (ii) breaking rapidly a rectangular rod in paraffine oil and keeping the resulting fractured surfaces in water for several days. The observation of these profiles reveals that the hydrogen concentration is important up to depths as large as 100 nm for fractured surfaces created under stress corrosion cracking, while it remains confined at the free surface – within the 10 nm depth resolution of the method – when the fractured surfaces were obtained under monotonic loading and exposed to moisture later. This clearly shows that water can enter into Silica glass during slow crack growth, and hence it is perfectly plausible that water

molecules react with Si-O bonds at a distance 100 nm from the crack tip within the bulk.

5. Conclusion

Ultra-slow crack propagation was observed in real time at the nanoscale through AFM in amorphous Silica. The main results from our observations are:

(i) Within the process zone, the crack tip does not propagate regularly, but through the growth and coalescence of damage cavities.
(ii) Velocity of the main CT and the cavity tips as measured at the damage zone scale are shown to be significantly smaller than the mean crack growth velocity as measured at the continuous scale. In other words, crack growth is intermittent and dominated by the accelerating phases corresponding to the cavity coalescence with the main CT.
(iii) The nanocavitation process provides the dominant mechanism responsible for damage spreading within the process zone.

Observations of damage cavities in amorphous Silica under stress corrosion are consistent to what was observed experimentally in Aluminosilicate glasses under stress corrosion (Célarié et al., 2003a, b; Marlière et al., 2003), and numerically during dynamic failure of amorphous Silica (Van Brutzel et al., 2002; Rountree et al., 2002; Kalia et al., 2003). This indicates that the existence of this nanoductile mode is inherent to the amorphous structure and does not depend on the precise glass composition.

The origin of cavitation should be found in the intrinsic toughness fluctuations induced by the amorphous structure of the material. This results in low toughness region sites and/or low density regions that behave as stress concentrators and give birth to cavities ahead of the main crack tip. Such a scenario was shown to capture quantitatively the cavity size at coalescence and the process zone extension in both the dynamic fracture simulations and the stress corrosion experiments.

This failure mechanism through growth and coalescence of damage cavities is very similar to what is observed classically – albeit at other length scales – in a wide range of materials, e.g. aluminosilicate vitroceramics (Célarié et al., 2003a, b; Marlière et al., 2003), nanophase materials (Rountree et al., 2002; Kalia et al., 2003), metallic alloys (Paun and Bouchaud, 2003), PMMA (Ravi-chandar and Yang, 1997) and polymers (Lapique et al., 2002). We argue that such mechanism is generic to crack propagation – the main difference resides in the typical lengthscales over which cavities are observed. These lengthscales are controled by the typical size of the microstructure eventually modified through environmental assisted activated process like stress corrosion or fatigue. The aspect ratio of the cavities – much larger in glasses and quasi-brittle materials than in metallic alloys – reflects the ability of the material to deform irreversibly. Such a scenario may explain the puzzling similarities observed in the scaling properties exhibited by fractures surfaces in a wide range of materials (Bouchaud, 1997).

Let us finally add that the present study sheds light on the role of the *spatial* fluctuations induced by the material microstructure, but passes over the *temporal* fluctuations in silence. Interaction of a growing crack with the material microstructure results in the release of acoustic waves (Ravi-chandar and Knauss, 1984; Bonamy and

Ravi-chandar, 2003, 2005) which play a significant role in the energy dissipation properties within the process zone. Their understanding represents interesting challenges for future investigations.

Acknowledgements

We acknowledge Thierry Bernard for his technical support. We are also indebted to Fabrice Célarié, Stephane Chapuliot, Rajiv Kalia, Christian Marlière, Laurent Van Brutzel, and Sheldon Wiederhorn for enlightning discussions, and to the MATCO programm for its constant support. CLR is currently supported by the National Science Foundation under Grant No. 0401467.

References

Barenblatt, G.I. (1962). The mathematical theory of equilibrium of cracks in brittle fracture. *Advances in Applied Mechanics* **7**, 55–129.

Bonamy, D. and Ravi-Chandar, K. (2003). Interaction of shear waves and propagating cracks. *Physical Review Letters* **91**, 235502/1–4.

Bonamy, D. and Ravi-Chandar, K. (2005). Dynamic crack response to a localized shear pulse perturbation in brittle amorphous materials: on crack surface roughening. *International Journal of Fracture* **134**, 1–22.

Bouchaud, E. (1997). Scaling properties of cracks. *Journal of Physics (Condensed Matter)* **9**, 4319.

Célarié, F., Prades, S., Bonamy, D., Ferrero, L., Bouchaud, E., Guillot, C. and Marlière, C. (2003a). Glass breaks like metal, but at the nanometer scale, Glass breaks like metal, but at the nanometer scale. *Physical Review Letters* **90**, 075504/1–4.

Célarié, F., Prades, S., Bonamy, D., Dickelé, A., Bouchaud, E., Guillot, C. and Marlière, C. (2003b). Surface fracture of glassy materials as detected by real-time atomic force microscopy (AFM) experiments. *Applied Surface Science* **212**, 92–96.

Dugdale, D.S. (1960). Yielding of sheets containing slits. *Journal of the Mechanics and Physics of Solids* **8**, 100.

Guilloteau, E., Charrue, H. and Creuzet, F. (1996). The direct observation of the core region of a propagating fracture crack in glass. *Europhysics Letters* **34**, 549–553.

Guin, J.P. and Wiederhorn, S.M. (2004). Fracture of Silicate Glasses: Ductile or Brittle? *Physical Review Letters* **92**, 215502/1–4.

He, M.Y., Turner, M.R. and Evans, A.G. (1995). Analysis of the double cleavage drilled compression specimen for interface fracture energy measurements over range of mode mixities. *Acta Metallurgica Materialia* **43**, 3453–3458.

Hénaux, S. and Creuzet, F. (2000). Crack tip morphology of slowly growing cracks in glass. *Journal of the American Ceramic Society* **83**, 415–417.

Inglis, C.E. (1913). Stresses in a plate due to the presence of cracks and sharp corners. *Transactions of the Institution of Naval Architects* **55**, 219–230.

Irwin, G.R. (1957). Analysis of stresses and strains near the end of a crack traversing a plate. *Journal of Applied Mechanics* **24**, 361–364.

Kelly, A., Tyson, W.R. and Cottrell, A.H. (1967). Ductile and brittle crystals. *The Philosophical Magazine* **15**, 567–586.

Kobayashi, T. and Shockey, D.A. (1987). A Fractographic Investigation of Thermal Embrittlement in Cast Duplex Stainless Steel. *Metallalurgical Transactions A* **18A**, 1941–1949.

Kalia, R., Nakano, A., Vashishta, P., Rountree, C.L., van Brutzel, L. and Ogata, S. (2003). Multiresolution atomistic simulations of dynamic fracture in nanostructured ceramics and glasses. *International Journal of Fracture* **18A**, 1941–1949.

Kurkjian, C.R., Gupta, P.K., Brow, R.K. and Lower N. (2003). The intrinsic strength and fatigue of oxide glasses. *Journal of Non-Crystalline Solids* **316**, 114–124.

Lapique, F., Meakin, P., Feder, J. and Jossang, T. (2002). Self-affine fractal scaling in fracture in ethylene and propylene polymers surfaces generated and copolymers, *Journal of Applied Polymer Sciences* **86**, 973–983.

Lawn, B.R. (1993). *Fracture of Brittle Solids* 2nd edn. Cambridge University Press, Cambridge.

Lawn, B.R., Hockey, B.J. and Wiederhorn, S.M. (1980). Atomically sharp cracks in brittle solids: an electron microscopy study. *Journal of Materials Science*. **15**, 12.

Marlière, C., Prades, S., Célarié, F., Dalmas, D., Bonamy, D., Guillot, C. and Bouchaud E. (2003). Crack fronts and damage in glass at the nanometre scale. *Journal of Physics-Condensed Matter* **15**, 2377–2386.

Miyamoto, H., Kikuchi, M. and Kawazoe, T. (1990). A study on the ductile fracture of Al-alloys 7075 and 2017. *International Journal of Fracture* **42**, 389–404.

Paun, F. and Bouchaud E. (2003). Morphology of damage cavities in aluminium alloys. *International Journal of Fracture* **121**, 43–54.

Prades, S., Bonamy, D., Dalmas, D., Bouchaud, E. and Guillot, C. (2005a). Nano-ductile crack propagation in glasses under stress corrosion: spatiotemporal evolution of damage in the vicinity of the crack tip. *International Journal of Solids and Structures* **42**, 637–645.

Proctor, B.A., Whitney, I. and Johnson, J.W. (1967). The strength of fused silica. *Proceedings of the Royal Society* **A297**, 534–557.

Ravi-Chandar, K. and Knauss, W.G. (1984). An experimental investigation into dynamic fracture-IV On the interaction of stress waves with propagating cracks. *International Journal of Fracture* **26**, 189–200.

Ravi-Chandar, K. and Yang, B. (1997). On the role of microcracks in the dynamic fracture of brittle materials. *Journal of the Mechanics and Physics of Solids* **45**, 535–563.

Rountree, C.L., Kalia, R.K., Lidorikis, E., Nakano, A., Van Brutzel, L. and Vashishta, P. (2002). Atomistic aspects of crack propagation in brittle materials: Multimillion atom molecular dynamics simulations. *Annual Review of Material Research* **32**, 377–400.

Swiler, T.P., Simmons, J.H. and Wright, A.C. (1995). Molecular dynamics study of brittle fracture in silica glass and cristobalite. *Journal of Non-Crystalline Solids* **182**, 68–77.

Tomozawa, M., Han, W.H. and Lanford, W.A. (1991). Water Entry into Silica Glass During Slow Crack Growth. *Journal of the American Ceramic Society* **74**, 2573–2576.

Van Brutzel, L. (1999). *Contribution l'étude des mécanismes de rupture dans les amorphes: étude par dynamique moléculaire de la rupture de verre de silice.* PhD Thesis, University of Paris VI.

Van Brutzel, L., Rountree, C.L., Kalia, R.K., Nakano, A. and Vashishta, P. (2002). Dynamic fracture mechanisms in nanostructured and amorphous silica glasses: million-atom molecular dynamics simulations. *Materials Research Society Symposium Proceedings* **703**, V.3.9.1–V.3.9.6.

Wiederhorn, S.M. (1967). Influence of water vapor on crack propagation in Soda-lime glass. *Journal of the American Ceramic Society* **50**, 407–414.

Wiederhorn, S.M. and Boltz, L.H. (1970). Stress corrosion and static fatigue of glass. *Journal of the American Ceramic Society* **53**, 543–548.